

Rapid assessment of earthquake-induced landsliding

Jonathan Godt (USGS) · Başak Şener (Middle East Technical University) · Kristine Verdin (USGS) · David Wald (USGS) · Paul Earle (USGS) · Edwin Harp (USGS) · Randall Jibson (USGS)

Abstract. We assess the likelihood of earthquake-induced landslides by combining global topographic data and geologic mapping with near-real-time estimates of ground shaking from large earthquakes. Results combined with global population estimates will provide emergency management with timely information on the possible societal effects of earthquake-induced landslides anywhere in the world. The distribution of topographic slope was calculated at 30-arcsecond spacing (roughly 1 km at the equator) using 3-arcsecond SRTM (Shuttle Radar Topography Mission) data. A global assessment of landslide susceptibility is used to assign material strength parameters in a one-dimensional limit-equilibrium slope-stability analysis to calculate threshold acceleration necessary to initiate landsliding. This assessment of potential instability is then combined with an estimate of strong ground motion provided operationally in the form of a “ShakeMap” by the U.S. Geological Survey National Earthquake Information Center. We apply this approach to two historical earthquakes, the 1976 moment magnitude (**M**) 7.6 Guatemala and 1994 **M** 6.7 Northridge, California earthquakes for which detailed landslide inventories are available. Results capture the broad spatial pattern of earthquake-induced landslides, but the quality of estimates is a function, in part, of the quality and resolution of the input data. We then apply the method to the recent **M** 7.9 earthquake in Eastern Sichuan, China to examine the probable spatial extent of landsliding from this event.

Keywords. Landslide, earthquake, ShakeMap

1. Introduction

Landslides are responsible for a significant part of the societal effects of large earthquakes in mountainous regions of the world (Keefer, 1984). Recent examples from Kashmir in 2005 (Owen et al., 2008) and Eastern Sichuan, China (Stone, 2008) highlight their direct effects in terms of human loss and damage to the built environment. Because of their impact on transportation networks, particularly mountain roadways, landslides often hinder emergency response efforts in remote areas. Less frequent, but of great potential consequence, are the temporary reservoirs impounded by large landslides that block stream channels (Costa and Schuster, 1988).

The U.S. Geological Survey’s (USGS) National Earthquake Information Center (NEIC) in Golden, Colorado, reports on more than 30,000 earthquakes a year, 25 of which cause significant damage, injuries, or fatalities. The Prompt Assessment of Global Earthquakes for Response (PAGER) system is designed to provide a near-real time estimate to governmental and non-governmental relief organizations, and the media of an earthquake’s effects anywhere in the world (Earle and Wald, 2007). One component under development is an estimate of the potential for earthquake-induced landslides. To that end we have applied methods developed

for regional landslide hazard zonation (e.g. Wieczorek et al., 1985; Jibson et al., 2000) to produce estimates of the likelihood of landslides resulting from large earthquakes in a global, automated manner. Similar efforts have been described previously (e.g. Mahadavifar et al., 2008) for regional assessment of earthquake-induced landslide occurrence.

2. Methods and Data

We apply a simplified Newmark (1965) stability analysis on a distributed basis using globally available geologic mapping and topography. Such analyses provide a critical or yield acceleration, a_c , above which ground acceleration is sufficient to overcome basal sliding resistance and initiate downslope movement,

$$a_c = (FS - 1)g \sin \alpha, \quad (1)$$

where FS is the static factor of safety, g , acceleration due to gravity, and α , the topographic slope angle in degrees (Newmark, 1965; Jibson, 1993). The static factor of safety is calculated using an infinite-slope stability analysis for a constant landslide thickness (2.4 m) neglecting the influence of groundwater. The critical acceleration is compared with the spatially distributed peak ground acceleration (PGA) delivered by the PAGER system using a modified “ShakeMap” approach (Wald et al., 1999). Newmark displacement is then estimated using the regression equation developed by Jibson (2007),

$$\log D_N = 0.215 + \log \left[\left(1 - \frac{a_c}{\text{PGA}} \right)^{2.341} \left(\frac{a_c}{\text{PGA}} \right)^{-1.438} \right] \pm 0.51 \quad (2)$$

where D_N is displacement in cm and the last term is the standard deviation of the model. We assume that estimated displacements exceeding 5 cm produce deformation that is potentially hazardous to people and the built environment (e.g. Wieczorek et al., 1985). In what follows we describe the global topographic and geologic databases used for model input.

Global topographic database

Shuttle Radar Topography Mission (SRTM) elevation data were used to create a globally complete slope dataset at 30-arcsecond resolution (Verdin et al., 2007). The SRTM elevation data are available globally at 3-arcsecond resolution (approximately 90 m at the equator), but the summary slope data layers were created at a reduced resolution of 30 arc-seconds. This resolution was chosen to be consistent with the ground-shaking estimates and the population datasets used in the PAGER system. Gaps in the SRTM data were filled using weighted scaling relations developed using the higher

resolution (1-arcsecond) National Elevation Dataset (NED) available for the United States and the globally complete GTOPO30 (30-arcsecond) dataset. Topographic slope was calculated in the steepest downslope direction accounting for the variation in cell spacing with latitude associated with data in geographic projection (see Verdin et al., 2007 for detailed description). The 30-arcsecond database consists of 15 data layers describing the distribution of elevation and topographic slope. The data layers used in the case study examples described below are the 1st, 10th, 30th, 50th, 70th, 90th, and 99th quantiles of topographic slope.

Global landslide susceptibility

We rely on a global landslide hazard evaluation presented by Nadim et al., (2006) to assign material strength properties to the land surface. Landslide susceptibility was estimated by ranking the map units that describe geologic age and lithology in a digitally available global geologic map (Hearn et al., 2003). For areas outside the United States the geologic database was compiled from existing 1:5M scale maps published by UNESCO (Hearn et al., 2003). Larger-scale geologic mapping is readily available for the continental United States (King and Beikman, 1974; Schruben et al., 1998) and Alaska (Beikman, 1980). We modified the Nadim et al., (2006) ranking to include several units in the highest susceptibility category and assigned friction angles and cohesion based on published values (e.g. Selby, 1993; Jibson et al., 2000) assigning the greatest material strengths to the least susceptible units in the modified ranking.

For the case study examples described in the next section, critical acceleration (eq. 1) and Newmark displacement (eq. 2) was calculated for each slope quantile. When combined, these calculations yield a spatial estimate of the likelihood of landsliding for a given level of ground shaking.

3. Case study examples

Guatemala 1976 magnitude 7.6

On 4 February 1976 a destructive earthquake struck eastern and central Guatemala killing more than 20,000 people and leaving nearly one fifth of the country's population homeless. Surface rupture along the Motagua fault extended for 230 km from the lower Motagua River valley to the west near Guatemala City (Plafker, 1976). The earthquake generated at least 10,000 landslides spread over an area of about 16,000 km² (Fig. 1A) concentrated in an area about 180 km west of the epicenter. Most were rock falls and debris slides of less than 15,000 m³ in Pleistocene-age pumice deposits, however several larger landslides were identified, some of which blocked stream drainages creating landslide dams that subsequently failed (Harp et al., 1981). Landslides triggered by the earthquake were responsible for several hundred deaths and disrupted transportation on several major highways and the national rail system.

Figure 1B shows the distribution of PGA estimated from available telesismic information since strong-motion instrumental records from the earthquake zone are not available. Visual comparison of the pattern of modeled landsliding with the mapped landslide inventory shows broad overall agreement (Figs. 1A and 1C), but some areas of localized concentration are only captured by the lowest likelihood estimates. For example, the dense area of landslides north of Guatemala City falls in the 1-10%

categories. We attribute this to the small scale of the geologic mapping and the uncertainty associated with the Guatemala ShakeMap. As stated previously, many of the landslides triggered by this earthquake were associated with young volcanic deposits that are not well mapped in this area in the global geologic dataset.

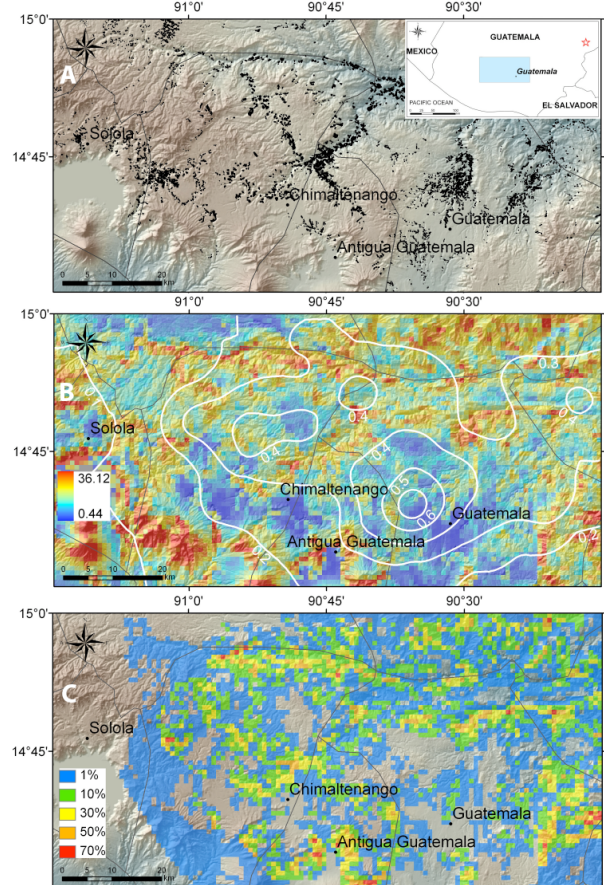


Fig. 1 Maps showing the landslides triggered by the M 7.6 Guatemala earthquake (A), PGA in g (contours) and median topographic slope (B), and estimated likelihood of landsliding (C).

Northridge 1994 magnitude 6.7

The 17 January 1994 Northridge, California earthquake caused widespread damage and estimated economic losses exceeding \$55 billion (2007 \$US; estimate from California Governor's Office of Emergency Services). Seventy-two people died as a result of the earthquake and many more were injured. The earthquake occurred at a depth of about 19 km on a blind thrust fault about 30 km northwest of Los Angeles and propagated northwest towards the ground surface (Wald et al., 1996). The earthquake triggered more than 11,000 landslides (Fig. 2A) over a 10,000 km² area (Harp and Jibson, 1995; 1996) most of which occurred in a 1000 km² area centered on the Santa Susana Mountains in the area of the largest permanent ground displacements (Wald et al., 1996). Most of the landslides were shallow (1-2 m thick) falls and slides of surficial materials overlying highly deformed Late Miocene through Pliocene-age marine and non-marine sedimentary rocks on slopes ranging from about 25 to 50

degrees (Jibson et al., 1994; Parise and Jibson, 2000).

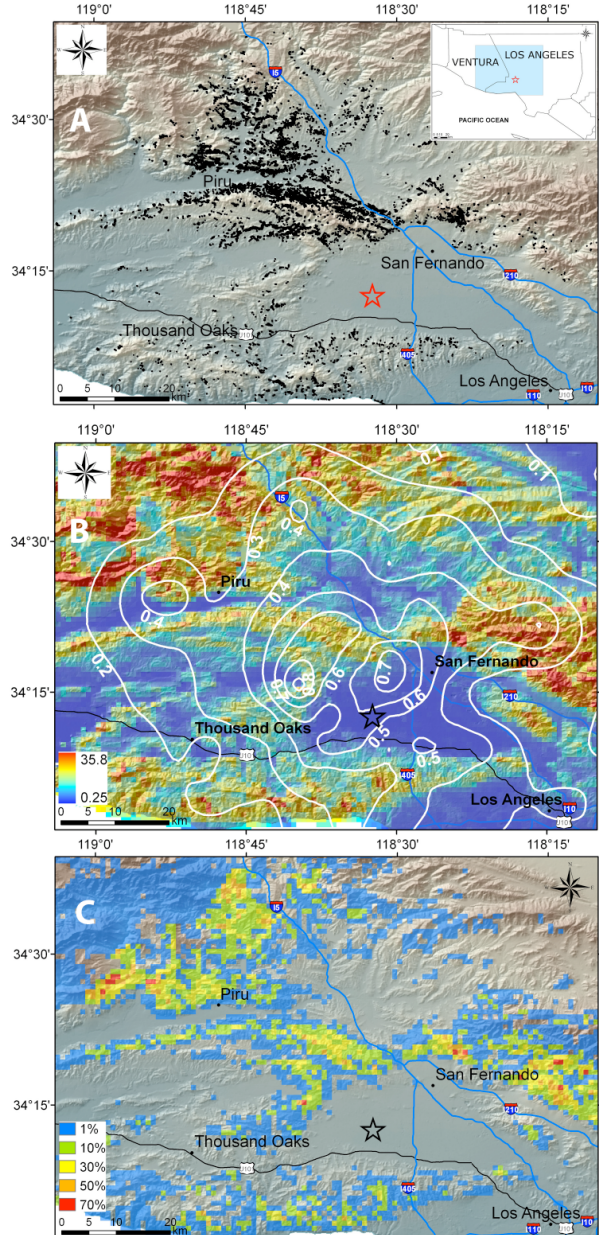


Fig. 2 Maps showing the landslides triggered by the M 6.7 Northridge, California earthquake (A), PGA in g (contours) and median topographic slope (B), and estimated likelihood of landsliding (C). The stars indicate location of the epicenter

Figure 2B shows the pattern of PGA associated with the Northridge earthquake created using instrumental data from several hundred strong-motion instruments (Wald et al., 1999). This better constrained distribution of ground shaking, compared to the Guatemala example, combined with the larger-scale geologic mapping (King and Beikman, 1974; Schruben et al., 1998) produce an improved estimate of landsliding (Fig. 2C). Visual comparison shows agreement between the broad spatial pattern of landsliding as well as

accurate identification of areas of concentrated landslides (Figs. 3A and 3C).

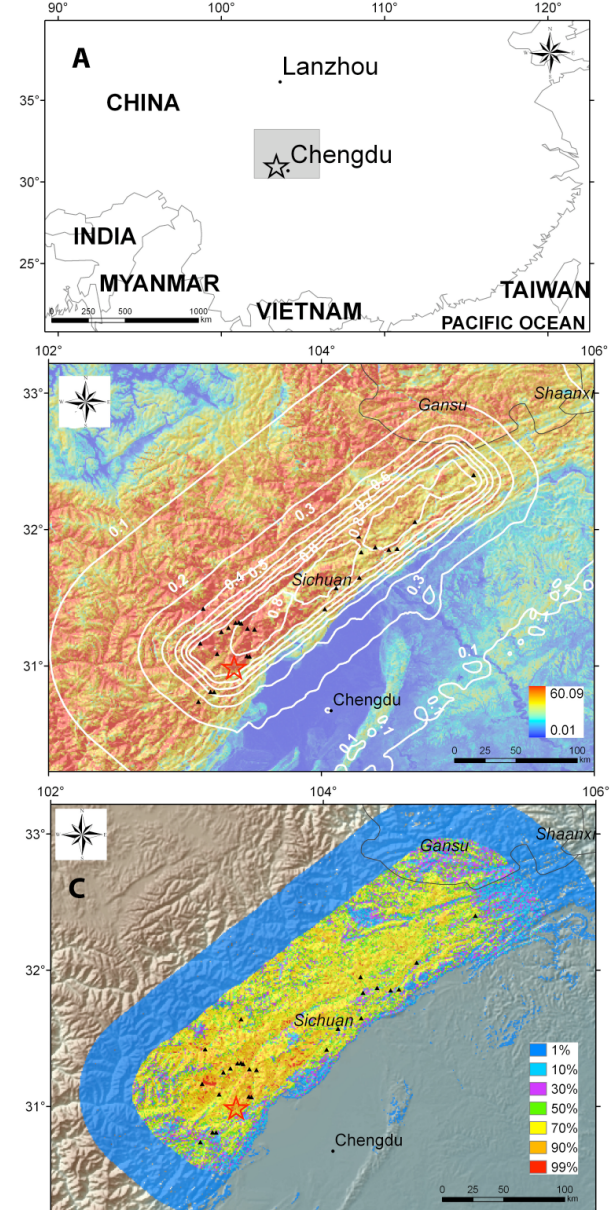


Fig. 3 Maps showing the location of the Eastern Sichuan, China study area (A), PGA in g (contours) and median, topographic slope (B), and estimated likelihood of landsliding (C). Black triangles indicate the location of landslide dams identified in imagery taken in late May of 2008. The stars indicate location of the mainshock epicenter.

Eastern Sichuan, China 2008 magnitude 7.9

The devastating earthquake on 12 May 2008 in Eastern Sichuan, China (Fig. 3A) occurred as the result of motion on a northeast striking reverse fault or thrust fault on the northwest margin of the Sichuan Basin (USGS-NEIC). Official figures of loss and damage include nearly 70,000 fatalities, several hundred thousand injured and more than 5

million left homeless. Tens of thousands of landslides were apparently triggered and more than 100 landslide dams were formed in this region of extreme relief on the margin of the Tibetan Plateau (Burchfiel et al., 2008; Stone, 2008). Figure 3B shows the distribution of PGA. Note that the region of very strong ground motion ($PGA > 0.5$ g) extends for several hundred km along the mountain range front and is in general coincident with the area of high landslide likelihood. To our knowledge, no landslide inventory is currently available, but we have identified the location of more than 20 large landslide dams, which are shown in Figure 3C and generally coincide with the areas predicted to have a high likelihood of landslides.

4. Concluding discussion

Near-real-time assessment of the societal impacts of large earthquakes in mountainous regions require some estimate of landslide occurrence. We present such an estimate using globally available digital topographic and geologic information. These data, combined with PAGER/ShakeMap, will provide a rapidly available, first-order assessment of the landslide potential following large earthquakes. Case-study results indicate that the quality of the ground-shaking estimates and the scale of geologic mapping have a substantial, but as of yet, unquantified influence on the accuracy of the estimates of the spatial extent and distribution of landsliding. Results are likely to improve as new, larger-scale, digital geologic mapping (i.e. OneGeology) and additional real-time strong motion data become available.

Acknowledgments

Mark Reid and Lynn Highland provided comments. B. Şener was supported by a grant from the Government of Turkey.

References

- Jibson, R. W. (1993) Predicting earthquake-induced landslide displacements using Newmark's sliding block analysis. *Trans. Res. Rec.* 1411, 9-17.
- Jibson, R. W. (2007) Regression models for estimating coseismic landslide displacement. *Eng. Geol.*, 91, 209-218.
- Jibson, R. W., E. L. Harp, and J. M. Michael (2000) A method for producing digital probabilistic seismic landslide hazard maps. *Eng. Geol.* 58, 271-289.
- Keefer, D. K. (1984) Landslides caused by earthquakes. *Geol. Soc. Am. Bull.* 95, 406-421.
- King, P. B., and H. M. Beikman (1974) Geologic map of the United States (exclusive of Alaska and Hawaii). *U.S. Geological Survey*, scale 1:2,500,000.
- Mahadavifar, M., M. K., Jafari, and M. R. Zolfaghari (2008) GIS-based real time prediction of Arias intensity and earthquake-induced landslide hazards in Alborz and Central Iran, in, *Landslides and Engineered Slopes: From the Past to the Future, Proc. of the 10th Int. Symp. on Landslides and Engineered Slopes, Xi'an, China*, Edited by Z. Chen, J. Zhang, Z. Li, F. Wu, and K. Ho, Taylor Francis Group, London, pp. 1427-1432.
- Nadim, F., O. Kjekstad, P. Peduzzi, C. Herold and C. Jaedicke (2006) Global landslide and avalanche hotspots. *Landslides* 3, 159-173.
- Newmark, N. M. (1965) Effects of earthquakes on dams and embankments. *Géotechnique* 15(2), 139-160.
- Owen, L. A., U. Kamp, G. A. Khattak, E. L. Harp, D. K. Keefer, and M. A. Bauer (2008) Landslides triggered by the 8 October 2005 Kashmir earthquake. *Geomorphology* 94, 1-9.
- Plafker, G. (1976) Tectonic aspects of the Guatemala earthquake of 4 February 1976. *Science* 193(4259), 1201-1208.
- Schruben, P. G., R.E. Arndt, and W. J. Bawiec (1998) Geology of the conterminous United States at 1:2,500,000 scale: A digital representation of the 1974 P.B. King and H.M. Beikman map. *U.S. Geological Survey Digital Data Series DDS-11*.
- Selby, M. J., (1993) *Hillslope materials and processes*. Oxford University Press, Oxford, UK, 451 pp.
- Stone, R. (2008) Scientists race against the clock to gauge landslide risk. *Science*, 320, 1408.
- Verdin, K. L., J. W. Godt, C. Funk, D. Pedreros, D. Worstell, and J. Verdin (2007) Development of a global slope dataset for estimation of landslide occurrence resulting from earthquakes. *U.S. Geological Survey Open-File Report 2007-1188*, 25 pp.
- Wald, D. J., V. Quitoriano, T. H. Heaton, H. Kanamori, C. W. Scrivner, and C. B. Worden (1999) TriNet "ShakeMaps": Rapid generation of peak ground motion and intensity maps for earthquakes in southern California. *Earthquake Spectra* 15(3) 537-555.
- Wald, D. J., T. Heaton, K. W. Hudnut (1996) The slip history of the 1994 Northridge, California earthquake determined from strong-motion, teleseismic, GPS, and leveling data. *Bull. Seismol. Soc. Am.* 86, 49-70.
- Wieczorek, G. F., R. C. Wilson, and E. L. Harp (1985) Map showing slope stability during earthquakes in San Mateo County, California. *U.S. Geological Survey Miscellaneous Investigations Series Map I-1257-E*. 1 Plate.